Solar Energy Materials & Solar Cells 248 (2022) 111982

Contents lists available at ScienceDirect

Solar Energy Materials and Solar Cells

journal homepage: www.elsevier.com/locate/solmat

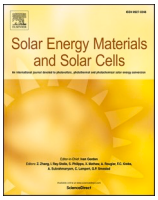

Epitaxial lift-off process for GaAs solar cells controlled by InGaAs internal sacrificial stressor layers and a PMMA surface stressor

Prabudeva Ramu *, Arto Aho, Ville Polojärvi, Timo Aho, Antti Tukiainen, Teemu Hakkarainen, Jarno Reuna, Jari Lyytikäinen, Roosa Hytönen, Mircea Guina

Optoelectronics Research Centre, Physics Unit, Faculty of Engineering and Natural Sciences, Tampere University, P.O. Box 692, FI, 33014, Tampere, Finland

A R T I C L E I N F O

Keywords:
Epitaxial lift-off
Quantum well
Thin-film solar cell
GaAs solar cell
Self-peeling
PMMA

A B S T R A C T

Epitaxial lift-off (ELO) techniques enable the development of thin-film III–V solar cell devices that are flexible and lightweight. To this end, we report an ELO process employing an internal sacrificial stressor layer (ISSL) and a surface polymer (PMMA) stressor layer. The combined action enhances the lateral etching rate and promotes a more controllable release process. The ISSL consists of quantum well-like GaInAs heterostructures that enable an accurate control of the stress required to enhance the lateral etching of the sacrificial layer, and hence the release of the thin film. More specifically, the use of the ISSL results in about 5-fold faster etch rate of the AlAs sacrificial layer. The ISSL layers can be etched away after the lift-off. Likewise, the PMMA surface stressor, which serves also as a sacrificial intermediate transfer layer, can be easily removed. The proof-of-concept device demonstration of the enhanced ELO technique was made by fabricating single-junction GaAs solar cells. The solar cell performance was evaluated under AM1.5d illumination and by external quantum efficiency measurements. Modelling based analysis shows that although the GaAs solar cell would require improvement of the front contact, yet the novel release process was successfully validated.

1. Introduction

Efficient and flexible solar cells are increasingly needed in a larger range of applications, including aerospace industry [1], automotive [2], or wearable photovoltaics [3]. At the same time, the flexibility and the higher power-to-weight ratio characterizing thin film solar cells are instrumental for the next generation space power systems [4]. While for terrestrial use there is a rather large portfolio of thin film solar cell technologies (e.g., silicon-based, CIGS, or perovskites), for space applications the choice of solar cell approach is largely limited to the use of III–V multi-junction architectures.

The performance of III–V solar cells has gradually increased over the years [5,6], reaching typical efficiencies of slightly more than 32% [7] for space operation, and up to 47% for terrestrial concentrator applications [8]. On the other hand, the development of thin-film III–V solar cells have been only marginally addressed, majority of the work being focused on the development of single-junction GaAs-based structures [9]. To this end, epitaxial lift-off (ELO) techniques have been developed with the primary drive being the cost reduction; using ELO to release the thin-film solar cell would enable to reuse the substrates, which is an important component of the solar cell materials cost [10,11]. Additional benefits are linked to the reduced thickness enabling a higher power-to-weight ratio, which is an important characteristic for aerospace industry [12]. Furthermore, thin-film architectures enable to deploy back-contact reflectors and implement advanced light trapping design leading to improved cell performance [13].

In general, the ELO process involves a sacrificial layer and a mechanism inducing an upward force promoting the release of the film. Established ELO techniques for GaAs solar cells involve AlAs or AlInP as sacrificial layers, while the upward force is typically induced via a weight-assisted process [14], or via surface-tension induced by the etching liquid [15].

The seed work on ELO technology dates back to 1978 when Konagai *et. al.* proposed a '*peeled film technology*' using the etching selectivity of HF acid for AlGaAs and GaAs [16]. Approximately 30 μm thick fragile thin-film could be thus released with a wax support layer after selective etching of AlGaAs. Later, Yablonovitch et al. realized that if the film structure was only a few micrometers thick, the wax support layer induces external stress to the layer stack and makes the resulted thin films to bend vertically promoting laterally etched underneath [17], as shown

* Corresponding author.
E-mail address: ramu.prabudeva@tuni.fi (P. Ramu).

https://doi.org/10.1016/j.solmat.2022.111982
Received 11 May 2022; Received in revised form 19 August 2022; Accepted 30 August 2022
Available online 8 September 2022

in Fig. 1. However, these processes suffered from limitations of a low etch rate as well as poor repeatability of the strain induced by the wax support layers. To alleviate these issues, Chancerel et al. exploited the internal strain inherent in the lattice mismatched AlAs release layers [18]. However, this modification has own limitation for multi-layer stacking related to strain-induced defects affecting the performance of the solar cell. In general, ELO processes require specific tools and structure dependent optimization of the sacrificial layer, etching, and the external force, aiming at attaining a good control of the bending process.

In this paper,we demonstrate a versatile ELO process, which we name i-ELO, which involves the use of internal strain induced via a double layer quantum-well (QW) InGaAs/GaAs structures. In addition, we use an external polymer stressor layer. The strain induced by the double layer internal structure can be designed to produce a controllable self-rollup during the i-ELO process for different layer structures.

2. Experimental

2.1. Preliminary i-ELO process

The GaAs-based structures were grown by VG Semicon V90 solid source molecular beam epitaxy (MBE) system on 3-inch diameter (100) n-GaAs wafers.

A first set of structures, shown in Fig. 2, were used to investigate the lateral etching rate of AlAs sacrificial layer without and with internal $In_{0.2}Ga_{0.8}As$ QWs stressor. The 15 nm QW layers are lattice mismatched by 1.43% with respect to GaAs. The corresponding compressive strain induces a self-rollup mechanism once the etching of sacrificial AlAs layer is initiated. The self-rollup was estimated by calculating the radius of curvature (ROC) after the AlAs etch using the equation B2 presented in Ref. [19] for calculating the wafer curvature for an arbitrary multilayer system.

For the ROC calculations we used a Poisson ratio of 0.31, which is considered appropriate for moderate lattice mismatch [20]. In addition, we used a Youngs modulus of 8.5331010 N/m^2 [19] while the plastic strain relaxation was neglected. The lattice constants for the calculations were calculated using values of the binary compounds in Vurgaftman et al. [21] and by using the Vegard's law for the ternary compounds. The structure and layer thicknesses are given in Figs. 2 and 6. It was also assumed that the ISSL layer is much thinner than the resulting thin film. By using this parametrization, the ROC of the film corresponding to the structure incorporating the ISSL was estimated to be 3.5 mm.

The etching was performed using either 50% Hydrofluoric acid (HF) or a mixture of Acetone (ACE) and 50% HF in the ratio of 1:1. The start and subsequent dynamics of the etch process is a rather complex mechanism being dependent on the flow of the etchants and removal of the etched products. Moreover, the etching dynamics depend on the mechanical behavior of the substrate and the peeling thin-film, which in the favorable case results in a self-rollup mechanism triggered by the strain affecting the two surfaces. In the absence of internal strain, the self-rolling process is triggered by the capillary tension induced by the etching liquid. Also, if the capillary tension is weak or there is not enough strain to sustain the roll-up effect, the ELO process can clamp and self-shutdown, as is schematically presented in Fig. 3.

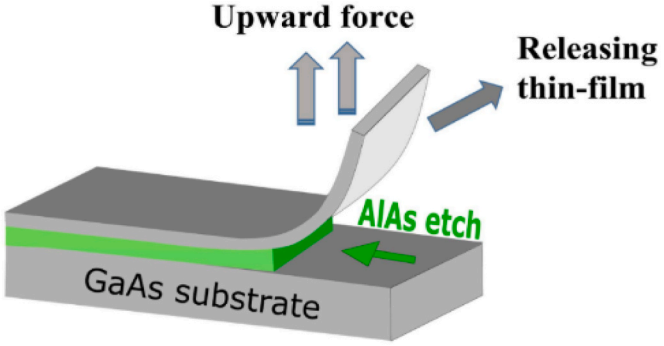

Fig. 1. Concept of a generic ELO process.

The etch rates, given in mm/min, for samples without and with strain layer are shown in Fig. 5. For the unstrained sample a higher etch rate was observed with HF and a slower etch rate was attained with a mixture of HF and ACE. However, we should also note that the HF concentration of the etchant solution could still play a role in controlling the lift-off process (see schematic description in Fig. 4).

This general picture explains the observed experimental dependence of the etch rate on the etchant mixture and internal strain shown in Fig. 5. The most important observation is that the samples including both strain layer and the 1:1 mixture of HF and ACE exhibit a 5-fold increase compared to the reference sample without internal stressor. Then for the sample with internal strain layers, the etch rate shows a further increase because of the surface tension of the etchant. Adding ACE to HF in the ratio of 1:1 lowers the surface tension of the etchant and permits larger concentration of fresh etchant ultimately to reach the reaction site thus increasing the etch rate [22]. This is opposite to the case without internal stressor where the bending is not sufficient, and etching is clamped (see Fig. 3).

2.2. Fabrication of GaAs solar cell via i-ELO

We should note, however, that the effect of the internal strain on the ROC, and hence on the etching rate, depends on the specific material composition of the film and its thickness. Therefore, the next set of samples studied were single-junction (1J) GaAs solar cell with a design shown in Fig. 6. While the general structure is typical for a 1J solar cells, it incorporates the AlAs sacrificial layer, the ISSL region for tailoring the internal strain, and also a GaInP etch-stop layer that was used for removing the ISSL heterostructure after i-ELO. Samples S1–S4 were different in terms of amount of strain induced (i.e.one or two InGaAs QWs) and thickness of the absorber (i.e. junction in Fig. 6). The estimated ROCs caused by internal strain and the main difference between the samples are summarized in Table 1.

The initial etching experiments with test samples having ISSL and GaAs layers described in Fig. 2 revealed sufficient bending for i-ELO process and transfer. However, similar ROC and ISSL values present in S1 full solar cell structure exhibit less bending for efficient i-ELO owing to increased total layers thickness. On the other hand, the S2 sample had a smaller ROC of 1.7 mm and was significantly thinner, which resulted in rolling up into a tube. Furthermore, S3 with double QW ISSL and 3 μm film thickness shows sufficient curvature for effective i-ELO whereas S4 having the maximum ROC with single ISSL lacks sufficient bending for reliable i-ELO.

In practice, for realizing full scale thin-film solar cell devices, it was found useful to deposit an external stressor layer of PMMA on the sample surface as shown in the concept Fig. 7. The use of the external polymer stressor in a controlled quantity compresses the thin film from the sides and further support the etching and lift-off. The polymer was found to experience partial swelling and shrinkage in the mixture of acid and solvent which induces external strain. This eventually controls the bending curvature by holding the released thin film intact during i-ELO.

Before the i-ELO process was initiated for the solar cell devices, a top p-type contact was deposited. This also ensured the mechanical support for the thin films after release. At this point we had to consider that metals can induce a compensating strain decreasing the bending curvature [23]. Moreover, the contact could also peel off due to poor adhesion on semiconductor. To this end we have tested several metal combinations and thicknesses and their compensating strain is measured using stylus profilometer. After several trials we have used a layer stack composed of 30 nm Ti, 30 nm Pt, and 300 nm Au. The metals were deposited by e-beam evaporation and exhibited good adhesion to the

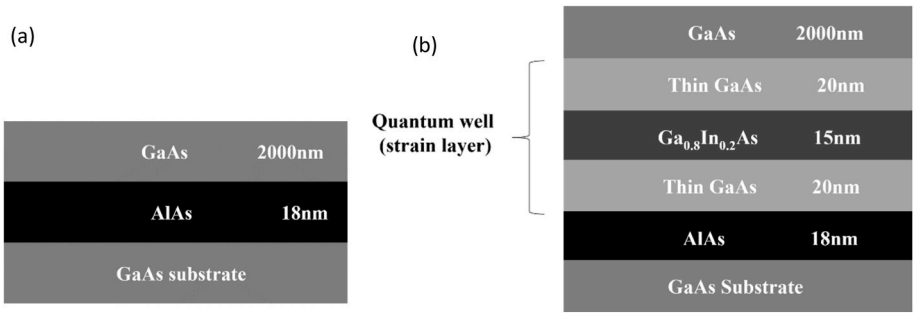

Fig. 2. Schematic of GaAs test structures. (a) without strain; (b) with strained QW layers.

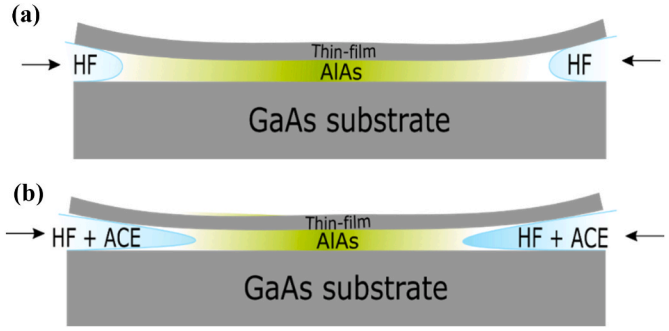

Fig. 3. Illustration of the etching dynamics in samples without internal strain and roll up of thin-film due to different surface tension of the etchant (a). HF with high surface tension (b). HF + ACE with reduced surface tension.

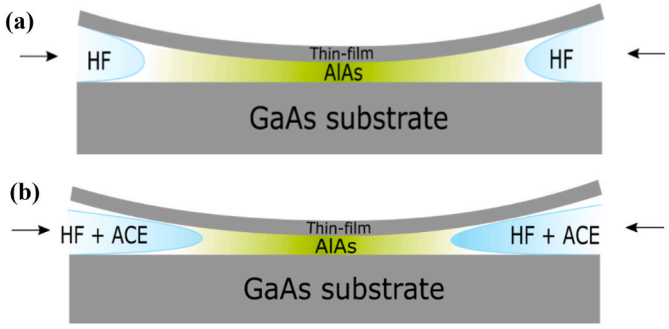

Fig. 4. Illustration of the etching dynamics in samples with internal strain (a). Showing limited flow of HF to the reaction site. (b). Showing the role of HF-ACE mixture to enhance/control the flow of the etchant to the reaction site.

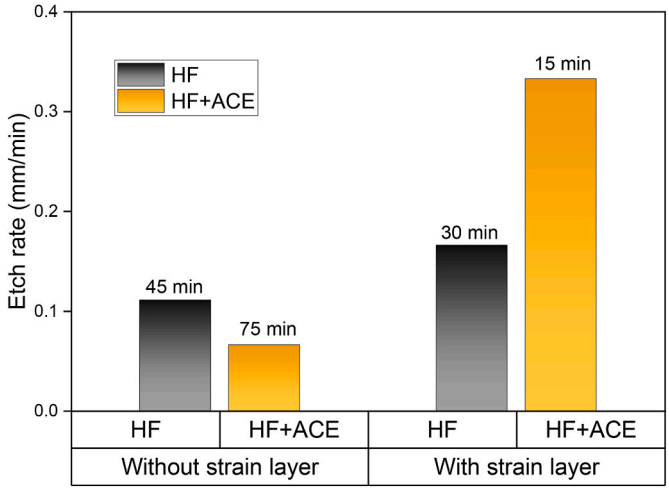

Fig. 5. Improved etch rates and the influence of strain layer in the lateral etching mechanism of ELO/i-ELO.

semiconductor film after i-ELO. The metal deposition step was followed by spreading of ~4.5 μl of PMMA stressor layer (applied to S3). Subsequently, the polymer layer was hard baked at 180 °C for 2 min and then the sample was immersed in HF:ACE until the AlAs layer was completely etched. The sample underwent i-ELO at an etch rate of ~15 mm/h. The achieved etch rate is almost 16 times faster compared to previously reported lateral etch rates of AlAs layer [24].

The curved thin-film remained on the substrate after release and the substrate was carefully lifted manually from the etchant. After the lift-off, PMMA was washed away with ACE before transferring the thin-film manually to a Kapton-on-glass carrier (see Fig. 8). The carrier substrate consists of double-sided Kapton tape bonded to a 160 μm thick glass plate. The curved thin-film released from the GaAs substrate was finally flipped over and pressed to the adhesive of Kapton-on-glass carrier. This manual transfer was carried out using a vacuum pen. When the thin film transfer process was properly and carefully done after, the thin-film solar cells were free of cracks and bends.

After the successful transfer, the strained double layers from the thin-film were etched away. Next, a top metal grid consisting of 10 nm Ni and 100 nm Au was deposited on n-side of the solar cell by e-beam evaporation through a shadow mask. Then we proceeded with mesa lithography and etching for electrical isolation. Etching of mesa through the whole semiconductor structure exposes back side metal contact on the p-side of the solar cell. The solar cell area was 5 mm × 5 mm. In the next step, the contact n-GaAs was removed and a double layer TiO2/SiO2 (50/89) nm anti-reflection coating (ARC) was deposited by e-beam evaporation.

The final step before device characterization is the wire bonding, which for a thin i-ELO structure is rather challenging if common processes for wafer based solar cells are used. In particular, it was found that direct wire bonding induces cracks at the bonding site and the crack lines extend through the thin-film. Therefore, the top and bottom contacts of the thin-film were connected with gold wires using bonding with silver epoxy glue.

3. Device characterization

External quantum efficiency (EQE) measurements were conducted using commercial Newport QuantX-300 system in the spectral range of 350 nm–1000 nm. The measured EQE characteristics of the solar cell prepared by i-ELO process are shown in Fig. 9 (data excludes the metal grid coverage). From the reflectance data it is apparent that the ARC is not optimal for this particular device; in fact, for wavelengths between 700 nm and ~900 nm the reflectance is ~10%. For the reflectance measurement one can see that the back surface reflector of this thin film solar cell composed of Ti/Pt/Au is far from optimal, since reflection for

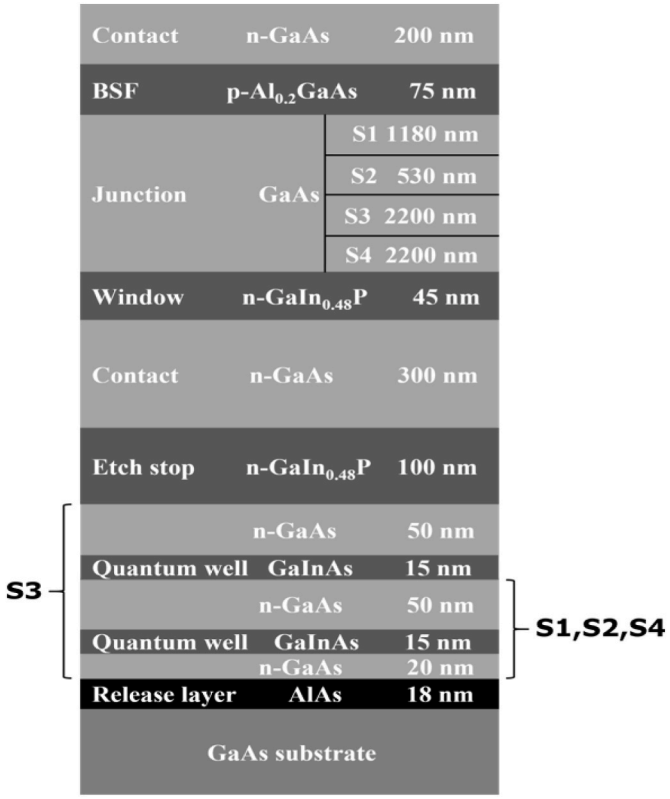

Fig. 6. Schematic of inverted-growth single junction GaAs solar cell structures with different junction thicknesses and ISSLs.

Table 1
Estimated Radius of curvatures corresponding to sample with different thicknesses and ISSLs.

ID	ROC	Film thickness	ISSL
S1	3.6 mm	2.0 μm	1 x InGaAs
S2	1.7 mm	1.3 μm	1 x InGaAs
S3	2.9 mm	3.1 μm	2 x InGaAs
S4	8.4 mm	3.0 μm	1 x InGaAs

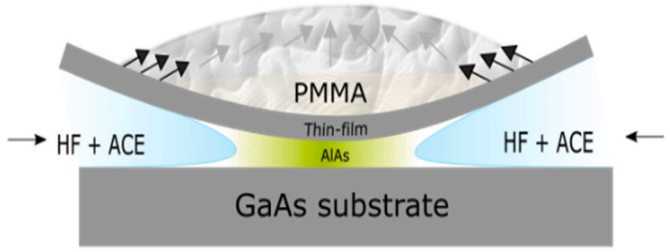

Fig. 7. Schematic illustration of i-ELO process with increased bending curvature influenced by the intermediate sacrificial layer PMMA.

over 900 nm is only 20% in average. The contribution of rather thick metal fingers is taken into account by measuring EQE with different number of the fingers under illumination and then extrapolating the data to zero fingers.

However, the rather high EQE value still indicates that the collection efficiency of generated photocarriers is high. Also, the dip in the EQE below 650 nm is due to the n-GaInP window layer that absorb some of the higher energy photons which then recombine at the surface. With enhanced window layer structure designing, the SC performance could be significantly enhanced for short wavelengths. In addition, with improved surface passivation the recombination process could be suppressed. The structure also does not contain an efficient back reflector that is known to enhance the long wavelength performance [25,26].

Furthermore, current-voltage (*I–V*) measurements were conducted using a 7 kW OAI Trisol Solar simulator that was set to ASTM AM1.5D (1000 W/m^2) spectral calibration. Moreover, the I–V characteristics of the thin film solar cell structure was also analyzed using PC1D software (version 5.9) [27,28]. The experimental *I–V* testing under AM1.5D simulated solar illumination and the PC1D simulation result are shown in Fig. 10. The short circuit current (J_{SC}) with wire bonding is significantly better than the direct measurement with the pins. We see that the direct pin measurement is too invasive for the thin-film yet the top contact function could be further engineered to operate adequately. The values of the key device parameters are: open circuit voltage of 978 mV, a J_{SC} of 23 mA/cm^2, a conversion efficiency of 16%, and a fill factor of 73%. Furthermore, the GaAs solar cell did not show any sign of shunt like behavior, which is an indication that the thin film structure does not contain processing-induced defects leading to current leak through the device.

As an experimental reference point for the *L–I–V* performance evaluation, we show also the *I–V* characteristics of an upright wafer-based GaAs solar cell that has the same structure, but is made on p-GaAs substrate, this solar cell does not have an ARC on it. Direct comparison shows that the V_{oc} values of the SCs match, being 965 mV for wafer-based SC. The thin film SC has even marginally better V_{oc} by 13 mV. In addition, the wafer-based GaAs SC is expected to have maximum J_{sc} of ~23 mA/cm^2 with a good ARC. Expected current generation and shunt free processing therefore has been clearly achieved for the i-ELO GaAs SC.

However, the cells exhibit quite high series resistance, the effect of which is studied by using PC1D simulations. The best fit between the measured and simulated *I–V* curves were obtained using a 5 Ω resistor in series with the solar cell. The series resistance component can originate either from the wire bonding method or it is directly related to top or bottom contacts. Our interpretation is that part of the excess resistance is most likely from the top metal contact of the solar cell connected to poorly conducting silver epoxy. By conducting separate *I–V* experiments for contact assessment, it was revealed that the epoxy/gold wire composite accounted for 1.4 Ω of the 5 Ω series resistance. Therefore, the i-ELO SC would benefit from some optimization of current spreading in the structure and improvement of contact properties. Improving the electrical contacts with minimized external resistance or even down to 1 Ω would greatly enhance the *I–V* characteristics, as shown in Fig. 10. In addition, due to the structure design, the photocurrent generation is absorption limited. For higher efficiencies either thicker junction or introduction of high-quality back surface reflectors are needed. Nevertheless, the *I–V* characterization reveals that our approach based on combination of ISSL and PMMA as an external stressor layer allows controlled ELO without a degradation of the solar cell structure. Therefore, the i-ELO process could be scaled up to a full wafer with profound understanding of the experiments and will be tested in the future.

4. Conclusion

We have devised a self-peeling ELO process based on the use of internally strained double layers to controllably affecting the lateral etching rate of the AlAs sacrificial layer. The use of the internal strain layers together with optimized etching chemistry and the use of a PMMA support layer resulted to improved thin-film structure release from the GaAs substrate. The EQE and electrical characteristics of the i-ELO processed GaAs solar cell indicated that no shunt component causing defects were generated during the fabrication process. The claim is supported by comparing the results to a wafer-based reference; the i-ELO cells show similar performance and even higher open circuit voltage. A high series resistance component found in *I–V* characteristics was

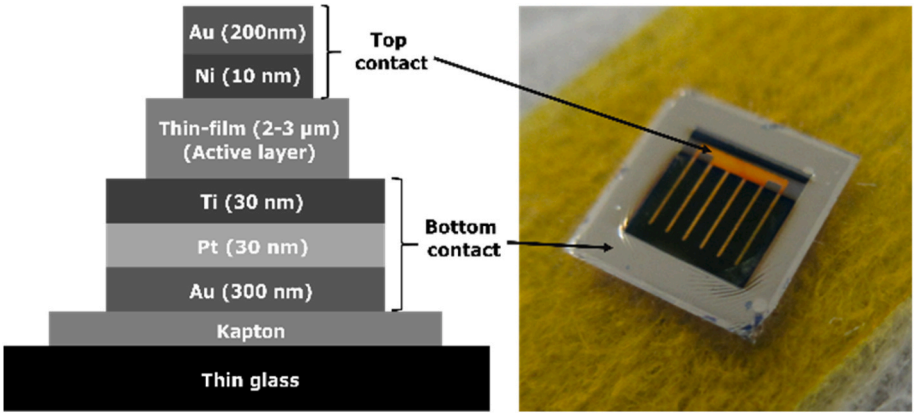

Fig. 8. Schematic illustration for the structure of i-ELO GaAs SC (left) and photograph of the processed i-ELO GaAs SC (right).

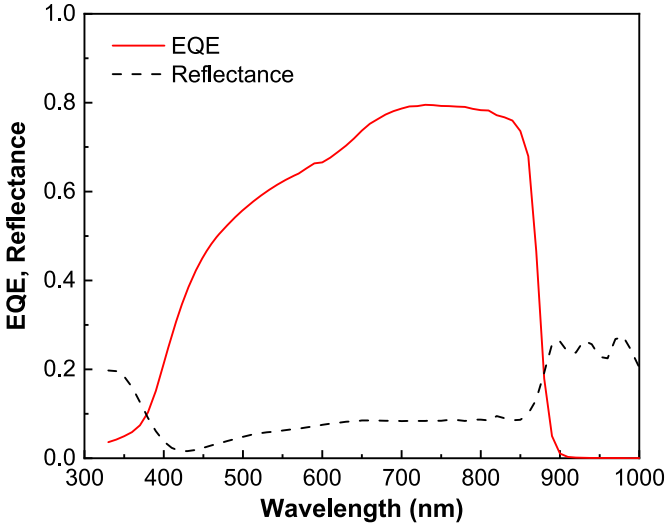

Fig. 9. Measured EQE and reflectance for the single junction GaAs solar cell calculated for zero finger coverage.

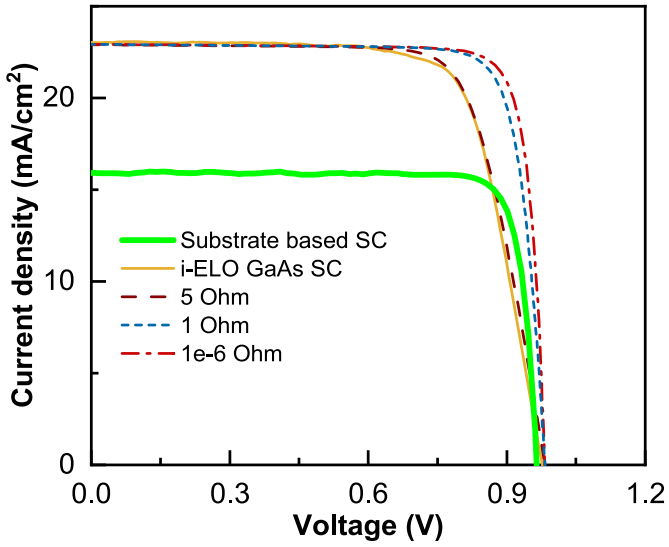

Fig. 10. Measured *I–V* characteristics of i-ELO solar cell with reference to the substrate-based cell. Simulated *I–V* characteristics with various series resistance values are also plotted.

associated to the bonding process with conducting silver epoxy. By improving the bonding process, employing backside reflectors, and optimized grid design, the device characteristics could be further improved.

CRediT authorship contribution statement

Prabudeva Ramu: Writing – original draft, Visualization, Methodology, Investigation, Formal analysis, Conceptualization. **Arto Aho:** Writing – review & editing, Project administration, Methodology, Investigation, Conceptualization. **Ville Polojärvi:** Writing – review & editing, Supervision, Methodology. **Timo Aho:** Supervision, Investigation. **Antti Tukiainen:** Writing – review & editing, Investigation. **Teemu Hakkarainen:** Methodology, Conceptualization. **Jarno Reuna:** Writing – review & editing, Investigation. **Jari Lyytikäinen:** Investigation. **Roosa Hytönen:** Investigation. **Mircea Guina:** Writing – review & editing, Supervision, Resources, Funding acquisition.

Declaration of competing interest

The authors declare that they have no known competing financial interest or personal relationships that could have appeared to influence the work reported in this paper.

Data availability

Data will be made available on request.

Acknowledgement

This work was supported by European Research Council (ERC AdG AMETIST, #695116). The work is also financially supported by Fortum and Neste Foundation Grant #20210054. In addition, the authors would like to acknowledge Arttu Hietalahti and Antti Fihlman for their technical support.

References

[1] Y. Kishi, H. Inoue, K. Murata, H. Tanaka, S. Kouzuma, M. Morizane, Y. Fukuda, H. Nishiwaki, K. Nakano, A. Takeoka, M. Ohnishi, Y. Kuwano, Ultralight Flexible Amorphous Silicon Solar Cell and its Application to an Airplane, N. p., Netherlands, 1991, https://doi.org/10.1016/0165-1633(91)90135-8.
[2] M.B. Schubert, J.H. Werner, Flexible solar cells for clothing, Mater. Today 9 (6) (2006) 42–50, https://doi.org/10.1016/S1369-7021(06)71542-5.
[3] Dhere, et al., CIGS2 thin-film solar cells on flexible foils for .pdf, 2002, https://doi.org/10.1002/pip.447.
[4] M. Yamaguchi, T. Takamoto, K. Araki, N. Ekins-Daukes, Multi-junction III-V solar cells: current status and future potential, Sol. Energy 79 (1) (2005) 78–85, https://doi.org/10.1016/j.solener.2004.09.018.

[5] R. King, A. Law, K. Edmondson, C. Fetzer, G. Kinsey, H. Yoon, R. Sherif, N. Karam, 40% efficient metamorphic GaInP/GaInAs/Ge multijunction solar cells, Appl. Phys. Lett. 90 (2007), 183516, https://doi.org/10.1063/1.2734507.
[6] J. Geisz, D. Friedman, J. Ward, A. Duda, W. Olavarria, T. Moriarty, J. Kiehl, M. Romero, A. Norman, K. Jones, 40.8% efficient inverted triple junction solar cell with two independent metamorphic junctions, Appl. Phys. Lett. 93 (2008), 123505, https://doi.org/10.1063/1.2988497.
[7] http://www.azurspace.com/index.php/en/products/products-space/space-solar-cells. Date viewed: 19th August 2022.
[8] J.F. Geisz, et al., Six-junction III–V solar cells with 47.1% conversion efficiency under 143 Suns concentration, Nat. Energy 5 (4) (2020) 326–335, https://doi.org/10.1038/s41560-020-0598-5.
[9] S. Moon, K. Kim, Y. Kim, J. Heo, J. Lee, Highly efficient single-junction GaAs thin-film solar cell on flexible substrate, Sci. Rep. 6 (2016) 1–6, https://doi.org/10.1038/srep30107. June.
[10] G.J. Bauhuis, et al., Wafer reuse for repeated growth of III-V solar cells, Prog. Photovoltaics Res. Appl. 18 (3) (2010) 155–159, https://doi.org/10.1002/pip.930.
[11] A. Van Geelen, P.R. Hageman, G.J. Bauhuis, P.C. Van Rijsingen, P. Schmidt, L. J. Giling, Epitaxial lift-off GaAs solar cell from a reusable GaAs substrate, Mater. Sci. Eng. B 45 (1–3) (1997) 162–171, https://doi.org/10.1016/S0921-5107(96)02029-6.
[12] D. Cardwell, et al., Very High Specific Power ELO Solar Cells (>3 kW/kg) for UAV, Space, and Portable Power Applications, 2018, pp. 3511–3513, https://doi.org/10.1109/pvsc.2017.8366552.
[13] T. Aho, et al., Back reflector with diffractive gratings for light-trapping in thin-film III-V solar cells, 2019 Eur. Sp. Power Conf. ESPC 2019-January (2019), 687253, https://doi.org/10.1109/ESPC47532.2019.9049262, 2019.
[14] J.J. Schermer, et al., High rate epitaxial lift-off of inGaP films from GaAs substrates, Appl. Phys. Lett. 76 (15) (2000) 2131–2133, https://doi.org/10.1063/1.126276.
[15] C.W. Cheng, K.T. Shiu, N. Li, S.J. Han, L. Shi, D.K. Sadana, Epitaxial lift-off process for gallium arsenide substrate reuse and flexible electronics, Nat. Commun. 4 (2013) 1577, https://doi.org/10.1038/ncomms2583.
[16] M. Konagai, M. Sugimoto, K. Takahashi, High efficiency GaAs thin film solar cells by peeled film technology, J. Cryst. Growth 45 (1978) 277–280, https://doi.org/10.1016/0022-0248(78)90449-9.
[17] E. Yablonovitch, T. Gmitter, J.P. Harbison, R. Bhat, Extreme selectivity in the lift-off of epitaxial GaAs films, Appl. Phys. Lett. 51 (26) (1987) 2222–2224, https://doi.org/10.1063/1.98946.
[18] F. Chancerel, et al., Epitaxial lift-off of InGaAs solar cells from InP substrate using a strained AlAs/InAlAs superlattice as a novel sacrificial layer, Sol. Energy Mater. Sol. Cells 195 (Jun. 2019) 204–212, https://doi.org/10.1016/J.SOLMAT.2019.02.013.
[19] T. Dieing, B.F. Usher, Wafer curvature in molecular beam epitaxy grown heterostructures, Phys. Rev. B 67 (2003), 054108, https://doi.org/10.1103/PhysRevB.67.054108.
[20] W.E. Hoke, T.D. Kennedy, A. Torabi, Simultaneous determination of Poisson ratio, bulk lattice constant, and composition of ternary compounds: in0.3Ga0.7As, In0.3Al0.7As, In0.7Ga0.3P, and In0.7Al0.3P, Appl. Phys. Lett. 79 (25) (2001) 4160–4162, https://doi.org/10.1063/1.1425954.
[21] I. Vurgaftman, J.R. Meyer, L.R. Ram-Mohan, Band parameters for III/V compound semiconductors and their alloys, J. Appl. Phys. 89 (2001) 5815–5875, https://doi.org/10.1063/1.1368156.
[22] F.-L. Wu, S.-L. Ou, Y.-C. Kao, R.-H. Horng, Separation-rate improvement of epitaxial lift-off for III-V solar cells, SPIE Newsroom 2015 (February 2015), https://doi.org/10.1117/2.1201501.005726.
[23] S.M. Analysis, et al., Making a Stress Measurement, 2010.
[24] F.L. Wu, S.L. Ou, R.H. Horng, Y.C. Kao, Improvement in separation rate of epitaxial lift-off by hydrophilic solvent for GaAs solar cell applications, Sol. Energy Mater. Sol. Cells 122 (2014) 233–240, https://doi.org/10.1016/j.solmat.2013.12.013.
[25] G.J. Bauhuis, J.J. Schermer, P. Mulder, M.M.A.J. Voncken, P.K. Larsen, Thin film GaAs solar cells with increased quantum efficiency due to light reflection, Sol. Energy Mater. Sol. Cells 83 (1) (2004) 81–90, https://doi.org/10.1016/j.solmat.2003.11.030.
[26] N. Gruginskie, et al., Increased performance of thin-film GaAs solar cells by rear contact/mirror patterning, Thin Solid Films 660 (2018) 10–18, https://doi.org/10.1016/j.tsf.2018.05.042.
[27] D.A. Clugston, P.A. Basore, PC1D version 5: 32-BIT solar cell modeling on personal computers, in: Proceedings of the 26th IEEE Photovoltaic Specialists Conference, 1997, https://doi.org/10.1109/PVSC.1997.654065.
[28] P.A. Basore, D.A. Clugston, PC1D Version 4 for windows: from analysis to design, in: Proceedings of the 25th, IEEE Photovoltaic Specialists Conference, Washington, 1996, pp. 377–381, https://doi.org/10.1109/PVSC.1996.564023.